UC Irvine
Faculty Publications

Title
Globally Gridded Satellite Observations for Climate Studies

Permalink
https://escholarship.org/uc/item/27h7340x

Journal
Bulletin of the American Meteorological Society, 92(7)

ISSN
0003-0007 1520-0477

Authors
Knapp, Kenneth R
Ansari, Steve
Bain, Caroline L
et al.

Publication Date
2011-07-01

DOI
10.1175/2011BAMS3039.1

Copyright Information

Peer reviewed

GLOBALLY GRIDDED SATELLITE OBSERVATIONS FOR CLIMATE STUDIES

by Kenneth R. Knapp, Steve Ansari, Caroline L. Bain, Mark A. Bourassa, Michael J. Dickinson, Chris Funk, Chip N. Helms, Christopher C. Hennon, Christopher D. Holmes, George J. Huffman, James P. Kossin, Hai-Tien Lee, Alexander Loew, and Gudrun Magnusdottir

As a calibrated and mapped geostationary satellite dataset, GridSat is easily accessible for both meteorological and climatological applications that allows a wide range of user-specified levels of sophistication.

With the recent passing of the fiftieth anniversary of the first U.S. weather satellite, questions on how to best use historical satellite data come to the forefront of the discussion on climate observation. There are now over 30 years of globally sampled geostationary and polar satellite data, and while the visible and infrared (IR) imaging instruments on the satellites were not specifically designed for climate purposes, the record has great potential to be used for observational climate studies. With this in mind, the National Oceanic and Atmospheric Administration (NOAA) recently embarked on an effort to derive climate data records (CDRs) from environmental satellite data (National Research Council 2004), including geostationary satellites. At present, most CDRs derived from historical satellites are based on polar-orbiting instruments, such as sea surface temperature data (Reynolds et al. 2002). Climatic use

AFFILIATIONS: Knapp, Ansari, and Kossin—NOAA National Climatic Data Center, Asheville, North Carolina; Bain* and Magnusdottir—University of California at Irvine, Irvine, California; Bourassa—Florida State University, Tallahassee, Florida; Dickinson*—Department of Earth and Atmospheric Sciences, The University at Albany/State University of New York, Albany, New York; Funk—USGS Center for Earth Resource Observations and Science, Santa Barbara, California; Helms* and Hennon—University of North Carolina Asheville, Asheville, North Carolina; Holmes—Department of Earth and Planetary Science, Harvard University, Cambridge, Massachusetts; Huffman—Science Systems and Applications, Inc., and NASA Goddard Space Flight Center, Greenbelt, Maryland; Lee—Cooperative Institute for Climate and Satellites, University of Maryland, College Park, Maryland; Loew—Max Planck Institute for Meteorology, KlimaCampus, Hamburg, Germany

*CURRENT AFFILIATIONS: Bain—Met Office, Exeter, United Kingdom; Dickinson—WeatherPredict Consulting, Wakefield, Rhode Island; Helms—The Florida State University, Tallahassee, Florida

CORRESPONDING AUTHOR: Kenneth R. Knapp, NOAA/National Climatic Data Center, 151 Patton Ave., Asheville, NC 28801
E-mail: ken.knapp@noaa.gov

of geostationary data has been limited largely to teams of satellite experts—for example, the international community activities of the Global Energy and Water Experiment (GEWEX) such as the International Satellite Cloud Climatology Project (ISCCP) and the Global Precipitation Climatology Project (GPCP).

Numerous issues hinder use of the complete global geostationary data record by the climate research community. First, each country archives its own geostationary data. Thus, to obtain global data, one could access data from the United States [for the Geostationary Operational Environmental Satellites (GOES)], Europe [for the Meteorological Satellites (Meteosat)], Japan [for the Geostationary Meteorological Satellites (GMS) and Multi-functional Transport Satellite (MTSAT)], and China [for the Feng Yun (FY) geostationary satellite]. Additionally, users might access geostationary data from other nations for climate studies, such as India, South Korea, and Russia. Second, the volume of full-resolution data can be unwieldy for any study at climate time scales. Third, the data format from each agency will be heterogeneous; furthermore, the data from any one agency may have multiple file formats. Assuming that users can overcome these hurdles, they must also calibrate (i.e., calculate radiances and brightness temperatures from the data) and navigate (i.e., determine the latitude and longitude for each image pixel) the data from each satellite.

As mentioned, the ISCCP and GPCP projects are two of the few climate uses of geostationary data prior to 2000. This is due in part to the international collaboration that overcame the hindrances described above. In doing so, the ISCCP stored a subset of satellite data at NCDC called ISCCP B1 that included data from each international meteorological satellite. However, necessary information about the data such as file format, navigation algorithms, and so on were not archived. This caused the ISCCP B1 archive to be mostly unusable until a rescue effort rectified these issues (Knapp et al. 2007) and provided access to the data for 1983–present. In addition, further efforts (Knapp 2008b) have expanded the period of record back to 1980.

The ISCCP B1 data have since been processed into Gridded Satellite (GridSat)

data, a format that is easily accessed and processed by the climate research community at large. This paper describes the construction of the dataset—describing some of the aspects of how the data are provided to facilitate user access—and highlights some of the applications of GridSat. Along the way, the reader is encouraged to consider GridSat not only as a resource for better understanding Earth's climate, but also as an example of how other observational data could be provided to a broad user community.

GRIDSAT OVERVIEW. GridSat data are derived from the ISCCP B1 data, which are detailed by Knapp (2008b). In short, the spatial, temporal, and spectral features of the data are similar to the Hurricane Satellite (HURSAT) dataset (Knapp and Kossin 2007), but at a global scale. The characteristics of the GridSat data are provided in Table 1. The data derive from full-disk images whose scans are closest to the synoptic times 0000, 0300, . . . , 2100 UTC. Primarily, image times begin within 15 min of the synoptic hour. When data from a synoptic hour are missing, the ISCCP project filled the gap with the best image available closest to that synoptic time.

The GridSat dataset is similar to the NOAA Climate Prediction Center (CPC) globally merged IR product, called the CPC-4km product (Janowiak et al. 2001). This product is created in real time and used to monitor global precipitation. Because of the similarity between GridSat and CPC-4km, the details of CPC-4km are provided alongside GridSat in Table 1. The primary difference between the two datasets is that the CPC-4km product is geared toward real-time weather and short-term climate applications whereas GridSat targets long-term global processing. For instance, both datasets attempt to reduce intersatellite differences by intersatellite normalization; however,

TABLE 1. Summary of similarities and differences between the CPC-4km product and the GridSat dataset.

	CPC-4km	GridSat
Spatial resolution	4 km	8 km
Temporal resolution	30 min	180 min
Channels	1 (IR)	3 (IR, water vapor, visible)
Monthly volume (uncompressed)	45 GB*	40 GB
Period of record	2000–present	1980–present
Intersatellite normalization	Yes	Yes
Temporal normalization	No	Yes
Format	Unformatted binary	netCDF

* 63 MB × 24 × 365.25/12 = 44.9 GB.

GridSat also performs temporal normalization via calibration against HIRS during the GridSat period of record. Thus, the data are complementary.

GridSat data are provided in an equal angle map projection (also called equirectangular or plate carrée), which facilitates the mapping and subsetting of the data. Since the ISCCP B1 native resolution is approximately 8 km, the resolution of the equal area grid is 0.07° latitude (~8 km at the equator). The data span the globe in longitude and range from 70°S to 70°N. The spatial and temporal coverage of the satellites contributing to ISCCP B1 is provided in Fig. 1—the so-called "geostationary quilt." The satellite intercalibration by Knapp (2008a) effectively stitches each quilt piece together, allowing for a consistent global dataset.

The satellites included in the GridSat are from agencies that contribute to the ISCCP project. While the first year of GridSat data (1980) is mostly composed of satellites in the *GOES-East* and *-West* positions (Fig. 1b), a four-satellite constellation is representative of the period from 1982 to 1998. (e.g., Fig. 1b). Failures of satellites often caused a three-satellite configuration but nearly global coverage is still possible (Fig. 1d), though at large view zenith angles. Finally, the Indian Ocean gap was filled in 1998, completing the global coverage (Fig. 1e). Figure 1a also demonstrates the international collaboration that resulted in satellite sharing to decrease data gaps, such as when *Meteosat 3* was moved west to increase coverage of the Atlantic Ocean in the early 1990s and when *GOES-9* was moved to the Pacific Ocean in 2003 to fill the gap between *GMS-5* and *MTSAT-1R*. In recent years, coverage has increased with the provision of the Chinese Feng Yun geostationary satellites and the loan of GOES for a South American coverage at 60° west.
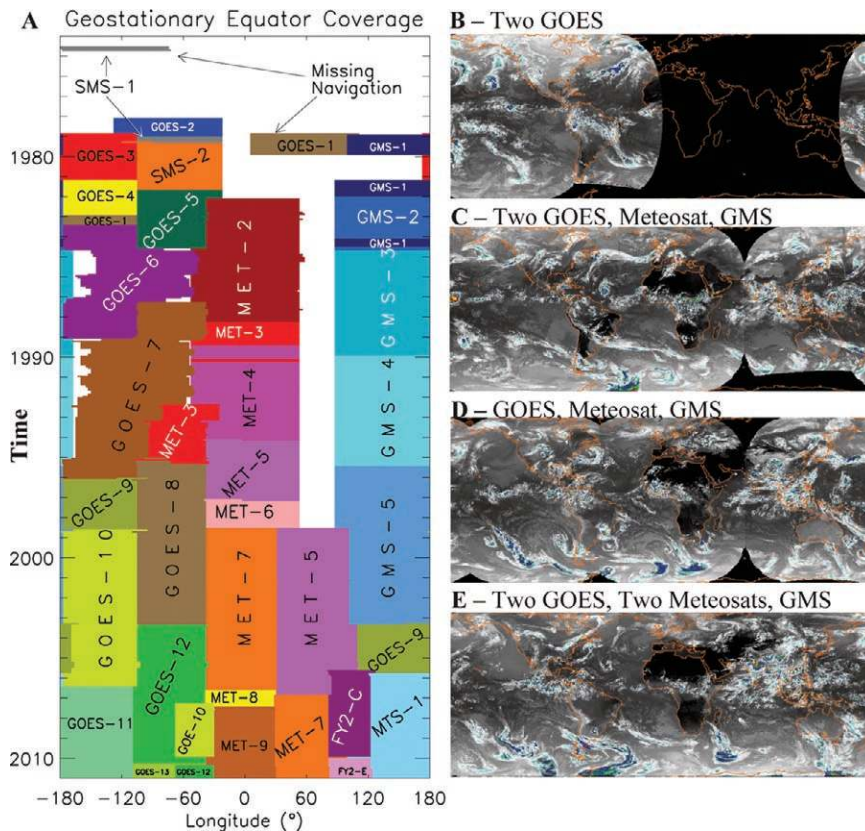

Fig. 1. (a) Time series of ISCCP B1 geostationary satellite coverage at the equator (limited to a view zenith angle of 60° for illustrative purposes. (b)–(e) Sample GridSat coverage for typical satellite coverages: (b) two-satellite coverage with only *GOES-East* and *-West* in 1980, (c) four-satellite coverage that is typical of most of the period 1982–98, (d) typical three-satellite coverage when the United States was operating only one satellite (e.g., 1985–87 or 1989–92), and (e) five-satellite coverage that is typical of the current era (1998–present).

GRIDSAT CHANNELS. In spite of the diversity of satellites and nations providing data, the ISCCP B1 data provide a uniform set of observations for the infrared window and visible channels—at 11 and 0.6 μm, respectively—during the period of record. Since 1998, the infrared water vapor channel near 6.7 μm is also available on a global basis.

The IR channel is a window channel (i.e., a spectral region with little atmospheric absorption) that senses Earth's surface under clear-sky conditions, cloud-top temperatures of thick clouds, and a combination of cloud and surface for optically thin clouds or broken clouds within a pixel. Many applications of this channel are discussed in the following paragraphs.

The visible channel is also a window channel that provides information on clouds and the surface. This channel also has the potential to provide information on Earth radiation budget variables such as aerosols (Knapp 2002) and surface albedo (Loew and Govaerts 2010).

The water vapor channels are generally centered near 6.7 μm, which is in a water vapor absorption band, making it sensitive to humidity in the upper troposphere. While GridSat water vapor data are temporally too sparse for most atmospheric motion vector applications (where operational products use 30-min data), it can still provide information on some circulation patterns.

INTERSATELLITE CALIBRATION. The data in GridSat use the intercalibration provided by ISCCP calibration efforts (Desormeaux et al. 1993) for the IR and visible channels. The IR channel has also undergone a second intercalibration using the High-Resolution Infrared Radiation Sounder (HIRS) channel 8 as a reference, which detected and corrected bias in the ISCCP calibration at cold temperatures after 2001 (Knapp 2008a).

The GridSat IR calibration uncertainty depends on the HIRS calibration as well as the observed differences between HIRS and the geostationary satellites. First, HIRS is a well calibrated and characterized instrument. Shi et al. (2008) estimate intersatellite differences for channel 8 to be less than 0.3 K. Furthermore, Cao et al. (2009) report that channel 8 is a good reference channel. Thus, if a sensor is calibrated against HIRS, it should be quite stable. Second,

based on the results of Knapp (2008b), the standard deviation of the monthly mean differences between ISCCP B1 and HIRS provides an estimate of monthly differences while the temporal trend of that bias provides an estimate of the long-term stability. In short, the GridSat IR calibration uncertainty is less than 0.5 K for any one satellite with a very stable temporal uncertainty that is less than 0.1 K decade^{-1}.

The water vapor channel calibration can be tied to a HIRS upper-level water vapor channel (band 12) but is complicated by the switch in central wavelength between HIRS/2 and HIRS/3 (from 6.7 to 6.5 μm) and is still being tested.

Data are calibrated and stored in GridSat files as brightness temperature (Tb) for longwave channels and reflectance for the visible channel. The IR data are calibrated following Knapp (2008a), view zenith corrected following Joyce et al. (2001), and parallax-corrected following Janowiak et al. (2001).

GRIDSAT PRODUCTION. For each 3-h time slot, the channels on each satellite are mapped to an equal-angle grid using nearest-neighbor sampling. Areas of satellite overlap are retained by storing data in layers (see Fig. 2). For each channel, the first layer retains observations with the nadirmost (i.e., lowest) view zenith angle, while a secondary layer holds the
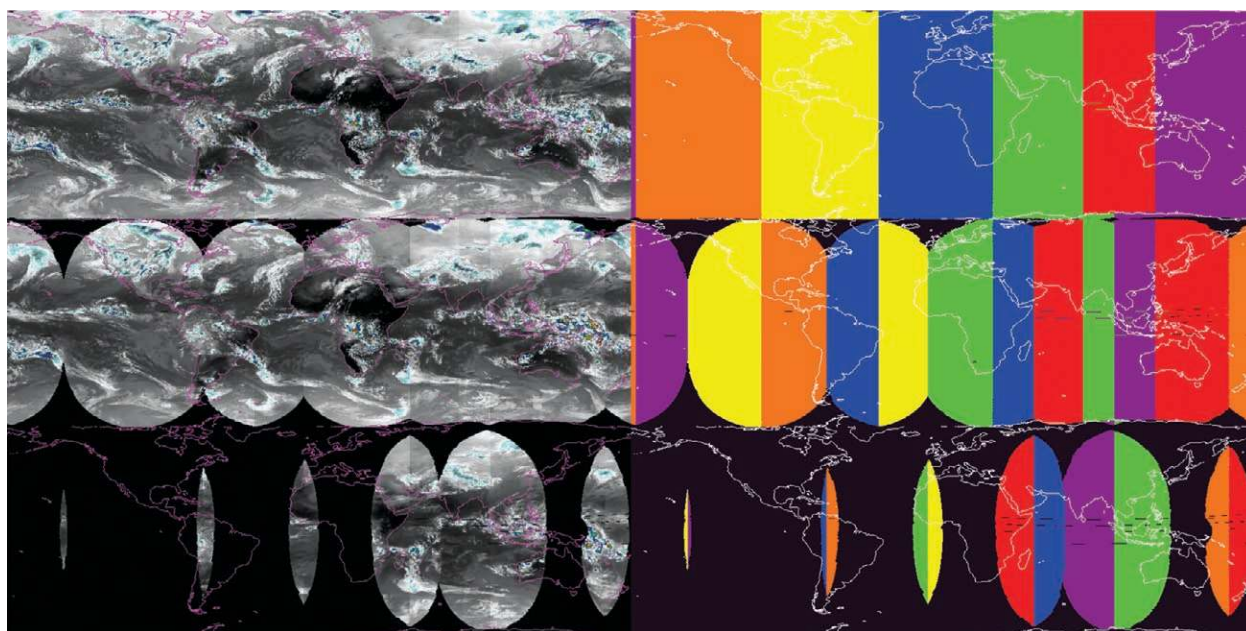

Fɪɢ. 2. (left) Merged GridSat IR image from 1 Jan 2008 and (right) identification of the satellites used to construct the IR image. The satellites *FY-2C* (red), *GOES-11* (orange), *GOES-12* (yellow), *Meteosat-7* (green), *Meteosat-9* (blue), and *MTSAT-1R* (violet) are used. Black regions denote missing data. The top row is the nadirmost set of observations. Observations and satellites in the second row are those not used in the top row because of larger view zenith angles. The third row consequently represents those observations eliminated from the second row.

regions dropped from the first layer. Similarly, a tertiary layer is retained for the third-best view zenith angles (which are dropped from the secondary layer). The extra layers are provided for future intercomparisons and intercalibrations (i.e., developing algorithms for various zenith angles). Furthermore, a satellite can be reconstructed by combining its contributions to each layer (e.g., by taking all the orange portions from each row of Fig. 2, one can reconstruct the *GOES-11* full disk image).

In addition to the channel data, satellite identification is stored per pixel with corresponding satellite information: satellite latitude, longitude, and radius. So while pixel-level satellite view zenith and azimuth angles are not stored, they can be calculated using the Earth location and the stored satellite position (e.g., Soler and Eisemann 1994). Furthermore, calibration information for each channel is provided such that original ISCCP B1 satellite counts can be backed out.

Data are stored using netCDF (Rew and Davis 1990) and the Climate and Forecasting (CF) metadata conventions, which facilitates usage with other software (see the sidebar "NetCDF and CF: Simplifying data access and processing"). Channel primary layers (nadirmost observation) are written as two-dimensional (2D) grids in the netCDF file, which facilitates processing of multiple files (e.g., aggregation of multiple times, etc.). Subsequent layers are written as either 2D grids or staggered arrays, which are one-dimensional arrays that only record data when they exist. Staggered arrays are more efficient when storing maps where data are mostly missing, as is often the case for the tertiary layer.

Finally, in keeping with National Research Council (2004), who recommend that the capability to reprocess data be incorporated as part of a climate data record program, the GridSat dataset can be reprocessed at NCDC. The entire period of record can be processed in about one week with current computing capabilities. So when new calibration coefficients, navigation adjustments or quality control (QC) algorithms are developed, the GridSat dataset has the capability to incorporate such improvements. At present, the GridSat data are updated annually, with a goal to update on a monthly basis.

DATASET APPLICATIONS FOR INFRARED WINDOW DATA. Here we present a selection of real-world climatological studies that depend on GridSat. The aim is to demonstrate the diverse nature of satellite data usage and emphasize the importance of historic satellite data to numerous scientific communities. The applications of GridSat described below are limited to the IR channel data, which has received more extensive intersatellite calibration. Many of these users are not satellite experts; their research would not have been completed in a timely manner without GridSat.

TROPICAL CYCLONES. Given the current questions regarding tropical cyclone (TC) variability in a warming climate and the challenges posed by the large uncertainties and heterogeneities in the historical tropical records, one very natural application of GridSat is toward the homogenization of these records.

Tropical disturbances and cyclogenesis. Tropical disturbances are early precursors of tropical cyclones. Traditionally, disturbances have been tracked and evaluated according to the Dvorak technique (Dvorak 1975, 1984), which estimates intensity based on the shape and evolution of cloud cover. This technique works best for systems nearing tropical cyclone stage; it is much less effective for weaker systems. To monitor weak systems, surface vector wind information can provide estimates of surface vorticity (Bourassa and McBeth-Ford 2010; Sharp et al. 2002), but coverage from a single scatterometer is insufficient to confidently track tropical disturbances. Therefore, Gierach et al. (2007) combined cloud-top IR observations with the surface vorticity to identify likely tropical disturbances, which proved to be effective for the North Atlantic basin and is being investigated for other tropical cyclone basins using GridSat.

Given the limited period of record of scatterometer data, another approach that uses only the IR data to detect potential tropical disturbances has been developed. One requirement for tropical cyclogenesis is the existence of a large area of intense and persistent thunderstorms, called a cloud cluster. Cloud clusters are associated with easterly waves, stalled midlatitude fronts, and large areas of atmospheric instability. Owing to their critical importance in the tropical cyclogenesis process, recent studies (e.g., Hennon and Hobgood 2003) have manually compiled large datasets of cloud clusters for analysis, a time-consuming task that involves individually examining thousands of basin-wide IR images.

In contrast, Hennon et al. (2011) use GridSat IR data to objectively identify cloud clusters, based on a definition by Lee (1989). The process uses a threshold to detect deep convection and then applies spatial and temporal constraints to determine if the convection is a cloud cluster. Figure 3 shows the frequency of

Recent advances in data services allow access and dissemination of data to a broad user community such that data servicing is now more than just putting files on an FTP server. Data servers provide numerous capabilities to users, for example allowing them to download only the data of interest, which saves download bandwidth and research time. Some of the capabilities are summarized below along with a real example of how data processing can be simplified with available tools.

NetCDF is supported by Unidata and has libraries that allow access to the data from dozens of programming languages. NetCDF version 4.1 also allows for data compression that results in smaller storage and bandwidth requirements. The GridSat data are stored in netCDF using the Climate and Forecasting convention. In doing so, GridSat data are stored in a manner that other tools recognize. In addition, tools such as the netCDF library and netCDF operators (NCO) (Zender 2008) are capable of reading files across the Internet without previously downloading the data.

GridSat data are served using the THREDDS data server (TDS) developed by Unidata, which allows users various options for downloading data. The TDS OPeNDAP access allows an OPeNDAP client (such as the NetCDF library, NCO, IDV and more) to remotely subset and download only the desired data slice or pixel. This provides efficient access to very large files or aggregations (i.e., virtual groups of files) without the user needing to download the entire dataset. The TDS Web Map Service access allows applications such as GIS, Google Earth, or online mapping to directly request rendered images (e.g., gif, png, jpeg) from the data server. These images already have a color table applied and can be produced in a variety of predefined projections. The TDS NetCDF Subset Service provides a web-based "slice-and-dice" service for users. Users may extract a spatial and temporal subset of the data and save the results as CF-compliant NetCDF, XML, or comma-separated variable (CSV) text files. Therefore, a variety of user access methods exist that provide interoperability with many existing software tools. Each method can be invoked by a single URL, enabling easy automation and scripting.

Numerous tools have been created to simplify the processing of CF compliant data. More than just data visualization, tools such as NCO provide command line capabilities to perform averages, concatenations, and more. For instance, sample code is provided in Fig. SB1 that processes one month of GridSat IR data, creating diurnally averaged IR Tb over the Sahara Desert for July 2002. Similar code was used to process the global diurnal cycle maps in the outgoing longwave radiation (OLR) section. The calls to NCO (*ncra* and *ncrcat*) provide a simple means to average IR Tb (via the −*v* flag) for a specific region (via the −*d* flag) and concatenate the files together. The alternative would be writing dozens of lines of source code (e.g., C or FORTRAN) to read in the data, calculate the diurnal average, define the output file, and write the data. Instead, the seven-line shell script accomplishes the same task. The resulting data can then be displayed easily with GrADS (using only four commands), for example, to show the mean temperature change from 0300 to 1500 UTC over the Sahara Desert (Fig. SB2).

In summary, it is clear that processing gridded netCDF data—such as GridSat—is simplified by the CF convention and the many tools available for serving and processing it.

```
#!/bin/bash

for hour in 00 03 06 09 12 15 18 21
do
  ncra GRIDSAT-B1.2002.07.??.$hour.nc \
      -d lat,10.,40. -d lon,-20.,45. -v irwin \
      -o GRIDSAT-B1.2002.07.$hour.nc
done
ncrcat GRIDSAT-B1.2002.07.??.nc -o GRIDSAT-B1.2002.07.nc
```

Fɪɢ. SB1. BASH code that uses netCDF operators to process one month of GridSat data of the Sahara Desert into diurnally averaged brightness temperatures.
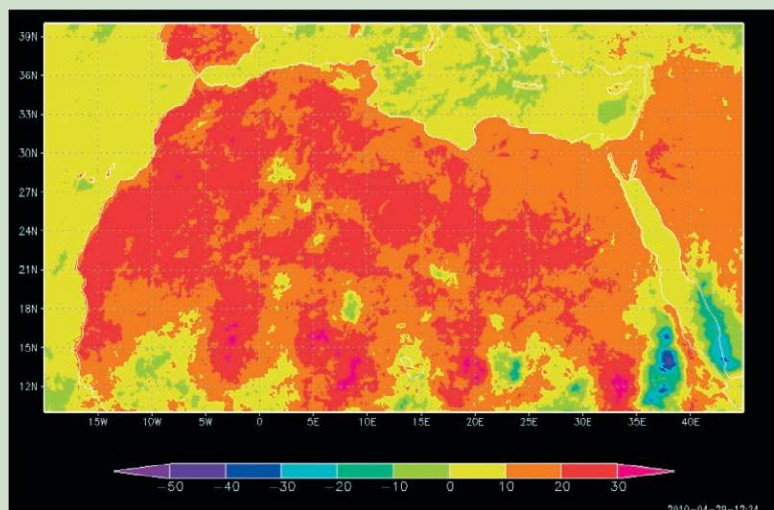

Fɪɢ. SB2. Average daily IR TOA temperature change (K) between 0300 and 1500 UTC over the Saharan Desert for August 2002.
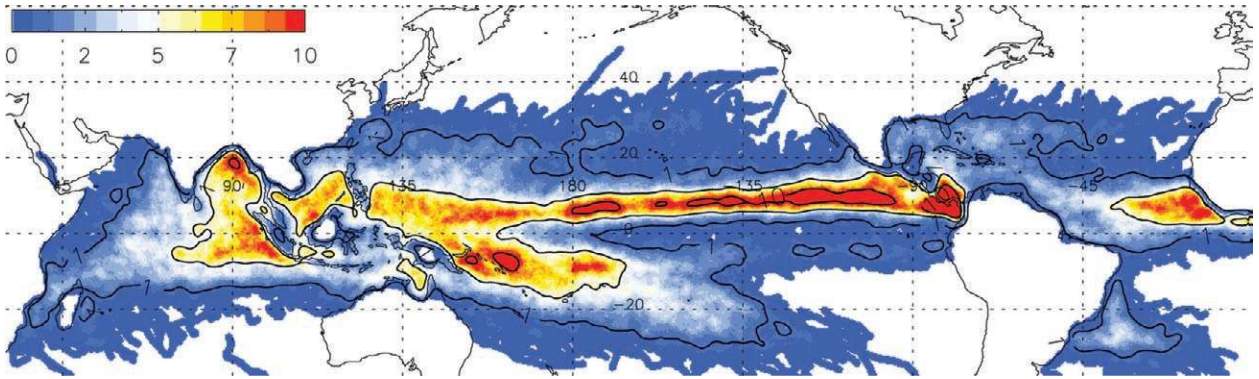
FIG. 3. Cloud cluster frequency (clusters per year within 55 km of any point) for the first decade of global satellite coverage (1998–2007). Contour levels are set at 1, 5, and 10 yr⁻¹.

objectively identified cloud cluster tracks for 1998–2007. The highest densities are found in the intertropical and South Pacific convergence zones, the North Indian Ocean, and off the west coast of Africa, consistent with observed areas of cloud cluster activity and tropical cyclogenesis. The complete cloud cluster dataset spans nearly 30 years and could be applied to several areas of research, including intraseasonal and interannual studies, impacts of climate change on cloud cluster activity, and case studies for use in tropical cyclogenesis research (e.g., using Knapp et al. 2010).

Estimating cyclone intensity and structure. Tropical cyclones are monitored and forecasted by a number of forecast agencies worldwide. Most forecast agencies provide estimates of the location and intensity of tropical cyclones in their areas of responsibility, but processes and data have improved over time. This makes the historical record of TC intensity heterogeneous by construction. Conversely, studies of the changes to tropical cyclone intensity require data with limited temporal heterogeneities. HURSAT data are the collocation of GridSat with tropical cyclones in the International Best Track Archive for Climate Stewardship (IBTrACS) data record (Knapp and Kossin 2007) (see Fig. 4). TC intensity reanalysis by Kossin et al. (2007b) using HURSAT suggests
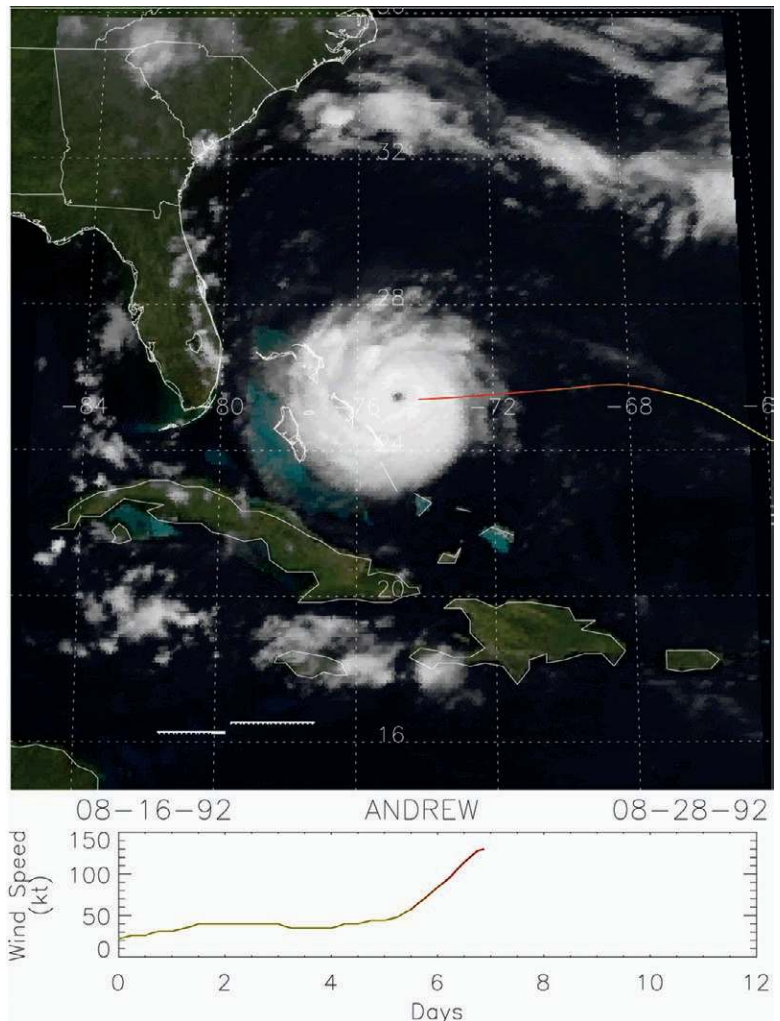

FIG. 4. HURSAT image of 1992 Hurricane Andrew from 23 Aug 1992 along with a time series of its maximum sustained wind (in knots).

that the trends in the original TC intensity record are inflated, likely due to changing procedures and capabilities. However, a significant upward trend in the intensity of the strongest storms is still present

after correction (Elsner et al. 2008). Additionally, the wind structure inside the tropical cyclone can be derived from HURSAT (Kossin et al. 2007a), providing information about the extent from the storm center that storm force winds reach.

Tropical cyclone transition to extratropical systems. Tropical cyclones moving out of the tropics to the midlatitudes can undergo significant structural and intensity modifications due to changes in the surrounding large-scale environment, a process termed extratropical transition (ET). In general, these tropical systems are weakening as they accelerate poleward over colder sea surface temperatures (or move over land) and into an increasingly baroclinic environment. The ET process is sensitive to the interaction of the decaying tropical cyclone with the atmospheric circulations and underlying ocean/land surface processes over midlatitudes (Jones et al. 2003). ET events can be tremendous rain makers as the large area of synoptically driven ascent can act on abundant tropical moisture. Numerous studies show that ET is common in all but the eastern Pacific Ocean (Foley and Hanstrum 1994; Hart and Evans 2001; Klein et al. 2000; Sinclair 2002). GridSat, via the HURSAT dataset, is being used to document in detail the remarkable events of late August 1992. During this period, the first ever documented ET in the eastern Pacific Ocean occurred: Hurricane Lester over the southwestern United States.

So in addition to the climatic perspective, GridSat data (via HURSAT) provide an understanding of tropical cyclone conditions throughout their lifetime.
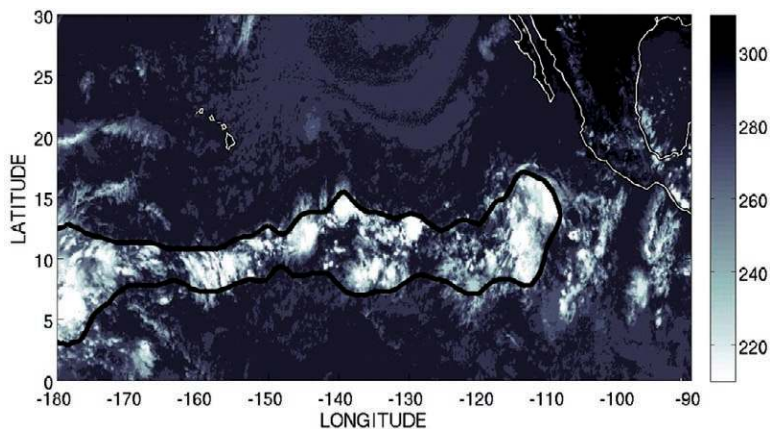

Fig. 5. Example of ITCZ detection in the eastern Pacific using the statistical model for 2100 UTC 18 Aug 2000. The grayscale represents IR temperature (K) from GridSat; the black line outlines the identified location of the ITCZ. The North American coastline is outlined in white.

DETECTION OF THE ITCZ AND ITS VARIABILITY ON DIFFERENT TIME SCALES.

GridSat's coverage in the tropics is ideal for the study of larger-scale weather features that may exceed the vision of a single geostationary satellite. The ITCZ is one such feature. It occurs as a narrow band spanning the tropics where the trade winds meet, and is visible as a region of increased convective activity. The transient nature of the ITCZ makes accurate detection for process studies challenging. Previous studies used analysis products (e.g., Magnusdottir and Wang 2008), manually labeled satellite frames (and therefore only use a few years of data; e.g., Wang and Magnusdottir 2006), or thresholded Tb to identify the ITCZ (Waliser and Gautier 1993). The latter has the disadvantage of including convection not associated with the ITCZ. Using GridSat data, Bain et al. (2011) developed a statistical model for ITCZ detection that objectively identifies the envelope of convection. The method requires that the satellite dataset be reliably calibrated over long periods and available at high temporal resolution. GridSat data are ideal for this approach. Figure 5 provides a snapshot of the objectively identified ITCZ in the east Pacific. The area inside the black curve represents the envelope of convection that the statistical model has determined is part of the ITCZ. Note that some isolated convection is not included as part of the ITCZ since it is determined not to be related to the larger-scale feature.

Using this technique, a database was created identifying the ITCZ in the eastern Pacific Ocean (0°–30°N, 90°W–180°) every 3 h from 1980 to 2008. The database has been used to construct detailed analysis of the variability of the ITCZ on interannual and intraseasonal time scales (Bain et al. 2011). The additional advantage of the high temporal sampling has also allowed in-depth studies of the diurnal cycle of the ITCZ (Bain et al. 2010), where the ITCZ size, as well as the character of clouds within in it, was found to vary according to time of day. The ability to use the same dataset for both short and long time scales lends strength to investigations of the ITCZ and is therefore particularly useful for relating climatological and dynamical aspects of the feature.

PRECIPITATION. The detection of precipitation is not wholly

unrelated to the above applications, as both tropical cyclones and the ITCZ can cause copious amounts of precipitation. The following details the study of precipitation using GridSat at global and regional scales.

Global precipitation climatologies. The Global Precipitation Climatology Project, an international community activity of GEWEX under the World Climate Research Program (WCRP), provides long-term global estimates of monthly and daily precipitation (Adler et al. 2003; Huffman et al. 2001). Previous and current GPCP algorithms use compilations of merged geostationary IR Tb whose period of record, latitudinal extent, and time/space resolution hamper computations. A new version of the GPCP datasets is now in development, with GridSat-B1 data as one key upgrade. Based on the contribution of GridSat, it is anticipated that the monthly product will be shifted from the current 2.5° grid to 0.5°, while the daily will shift from 1° to 0.25°. In addition, the daily dataset eventually could be pushed from its current start of October 1996, perhaps to the start of Special Sensor Microwave Imager data in July 1987. For both datasets, the current latitude bounds for geostationary IR data of 40°N–40°S will be relaxed to the entire useful range of simple IR-based estimates, around 50° in the summer hemisphere.

In addition to these traditional precipitation climatologies, GridSat also facilitates research on precipitation detection. For instance, GridSat provides complementary information at high temporal and spatial resolution for three different channels. The high spatial resolution of GridSat can help to better identify cloud systems capable of producing rain while the high temporal resolution allows for tracking the development and movement of medium- and large-scale cloud systems. The data from the IR channel can be used to better identify convective cells and therefore resolve precipitating systems with a scale smaller than the footprint of a microwave sensor [similar to the approach of Joyce et al. (2004)]. Merging the multispectral and high-resolution GridSat data with data from sensors on polar-orbiting satellites might be a fruitful pursuit, which could allow for temporal interpolation between subsequent overpasses of a microwave sensor that only provide a few observations per day at a global scale.

Erroneous discrimination of optically thin and thick clouds can have a significant effect on uncertainties in precipitation retrieval (Ba and Gruber 2001). Nonprecipitating cirrus clouds mistakenly interpreted as thick precipitating clouds contribute to overestimation of rain rate. Differencing between GridSat IR window and water vapor channels allows one to discriminate between optically thin clouds and thick clouds possibly overlaid by cold ice clouds (Turk and Miller 2005). Thus, GridSat data will likely have a significant impact on improved global precipitation climatologies.

Mercury wet deposition: Polluted rain. At regional scales, Holmes et al. (2008) and C. Holmes et al. (2011, unpublished manuscript) applied GridSat data to the study of societal impacts of precipitation in the eastern United States. Wet deposition is a major source of mercury to ecosystems, which can be harmful to fish, birds, and humans (Lindberg et al. 2007; Mergler et al. 2007; Scheuhammer et al. 2007). For example, fish in many U.S. water bodies have mercury concentrations considered unsafe for consumption, motivating efforts to understand and reduce mercury exposure through precipitation.

Mercury deposition in the southeast United States is nearly double that in the northeast (Fig. 6a) despite lower anthropogenic emissions in the region (Environmental Protection Agency 2008; Mercury Deposition Network 2006). Peak seasonal deposition occurs in summer when convective storms are common. This led Guentzel et al. (2001) and Selin and Jacob (2008) to hypothesize a causal link between high-altitude wet scavenging in deep convection and the elevated deposition. Holmes et al. (2008) and C. Holmes et al. (2011, unpublished manuscript) tested this hypothesis by correlating IR cloud temperatures from GridSat with mercury deposition measured by the EPA Mercury Deposition Network (MDN). Precipitation samples accumulate over one week and the associated cloud temperatures are calculated as the average over the collection period of daily minimum temperatures observed within 20 km of the collection site. Deposition clearly increases with colder temperatures (Fig. 6b), but this is partially due to large precipitation depths associated with tall, cold clouds. Figure 6c shows that even for equivalent rainfall depths, mercury deposition is about 2 times greater in the samples with the coldest average clouds ($Tb < 240$ K) compared with the warmest ones ($Tb > 260$ K). Ongoing work addresses the dynamical implications of these results.

PRECIPITATION AND TEMPERATURE MONITORING IN DATA-SPARSE REGIONS.
Another societal implication of precipitation is the availability of food production in regions with little irrigation infrastructure, where adverse trends in
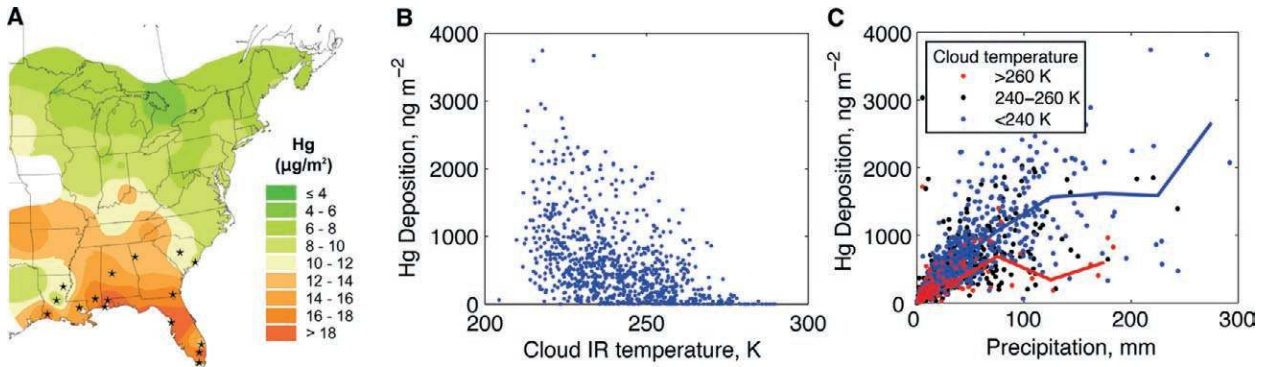
Fig. 6. (a) Mercury wet deposition in the eastern United States for 2005. Stars show sites analyzed here. (b) Mercury wet deposition for summers 2001–06 and mean IR cloud temperature from GridSat IR. (c) Mercury wet deposition and precipitation for three different cloud temperature ranges. Lines show mean concentration in 50-mm precipitation bins for the coldest (temperature < 240 K) and warmest (temperature > 260 K) clouds. [Figures adapted from Holmes et al. (2008) and C. Holmes et al. (2011, unpublished manuscript); Mercury Deposition Network 2006.]

rainfall and temperature can disrupt agriculture and pastoral livelihoods. Our understanding of where rainfall declines or temperature increases exacerbate food security has been limited by sparse in situ data. Therefore, the U.S. Agency for International Development Famine Early Warning Systems Network (FEWS NET) has supported the creation and analysis of rainfall and temperature climatologies in food-insecure regions. FEWS NET has begun working extensively with the GridSat data in order to make finer-resolution maps of rainfall and air temperatures over a 30-yr period.

Spatial analysis of GridSat IR Tb percentiles are used over a 4-month period to estimate mean temperature and total precipitation based on correlation with the sparse in situ sites. For algorithm details, see Funk et al. (2011).The mean 1999–2008 June–September (JJAS) temperature field is in the top left of Fig. 7.

High mountainous areas in Kenya, Ethiopia, and near the border of Cameroon and Nigeria are cool, while the sands of the Sahara and the Afar region of Ethiopia are very warm. Long-term variations can be mapped by looking at decadal differences (between two decades: 1984–93 and 1999–2008).

Looking at the temperature changes (Fig. 7, bottom left), a substantial warming signal is apparent, which also appears in the station data. Spatially, however, the strongest warming (>1°C since 1984–93) appears across a coherent area stretching from western Kenya and Ethiopia across the Zaire basin. June–September rainfall, on the other hand, exhibits an increase across northern Ethiopia and most of the Sahel. Decreases are found across eastern Ethiopia, most of Kenya and Uganda, and the Zaire basin. The spatial detail of these maps should help us understand and adapt to decadal climate variations. Such differences may
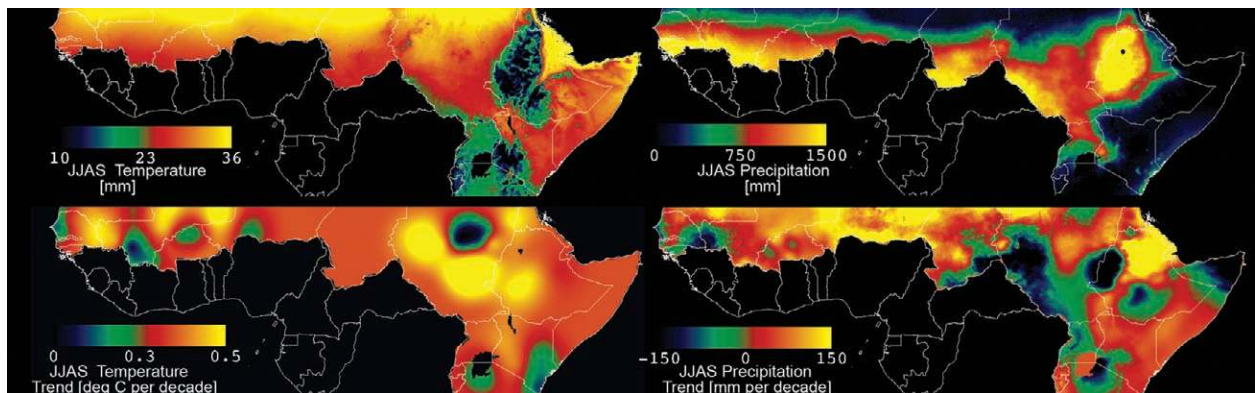

Fig. 7. JJAS air temperature and rainfall estimates based on combinations of GridSat infrared fields and in situ station observations. The top two panels show decadal average (left) air temperature and (right) rainfall for the 1999–2008 period. The bottom panels show the differences between these decadal averages and the 1984–93 average (the 1999–2008 average minus the 1984–93 average).

relate to climate change or may be simply due to inherent climate variability. In either case, decadal fluctuations can impact food security, hydrological resources, and environmental sustainability. The GridSat data help us capture shifts in temperature and precipitation, building a high-resolution picture of change. While the GridSat-enhanced analyses are still evolving, it seems likely that these data will substantially improve our ability to track rainfall and temperature changes, enhancing our ability to adapt in a changing world.

OUTGOING LONGWAVE RADIATION.

The Earth radiation budget describes the distribution of radiative energy in the Earth–atmosphere system. The observations of Earth radiation budget parameters at the top of the atmosphere have been performed from both operational and experimental satellites since the 1970s. The long and continuous time series of Earth radiation budget parameters (e.g., the OLR) is valuable for climate change studies and monitoring. Polar-orbiting satellites provide fairly uniform spatial and angular sampling from a given instrument, but with relatively poor temporal sampling resolution. GridSat data provide information on the diurnal variation that is essential for deriving the OLR time series accurately.

The HIRS OLR climate data record was generated with a set of climatological OLR diurnal models (Lee et al. 2007) that help to reduce the monthly OLR errors resulting from the orbital drift of polar-orbiting satellites. Although these models are self-consistent with the HIRS OLR retrievals, for error budgeting purposes we would like to assess whether these diurnal models were truly representative and how significant the interannual variations can be. Figure 8 shows the comparison of the HIRS climatological OLR diurnal models for August 2002 with those derived from the GridSat IR data. Some disagreements are apparent for certain regions/climate types. Nevertheless, for the majority, they seem to share a high degree of similarity, both in shape and in phase. These results provide us confidence in the quality and guidance for future improvement of the OLR climate data record production. Similar comparisons are necessary for other seasons and years.

A hybrid OLR product can then be generated using HIRS observations and GridSat following Lee et al. (2004). Such a combination would take advantage of both the accuracy of the HIRS OLR retrieval and the precise diurnal variation signal in GridSat. This product will improve the temporal integral accuracy for the HIRS climate data record and possibly allow product generation at a temporal resolution finer than monthly, which would benefit dynamical diagnostic applications.

FUTURE WORKFUTURE APPLICATIONS USING VISIBLE AND WATER VAPOR CHANNELS. The bulk of the above applications focused on the IR channel; however, many areas of study exist for the global intercalibrated visible and water vapor channels. The visible channel is sensitive to clouds and in some regions aerosols as well. Aerosols have a significant role in our daily lives by affecting human health and in our understanding of Earth's radiation budget via the uncertainty in how much solar radiation they reflect to space versus absorb (in addition to how they affect cloud optical properties and lifetime). Knapp (2002) defined a means to detect the aerosol signal in satellite observations. When this technique is applied to visible GridSat data, many ground sites—Aerosol Robotic Network sites (Holben et al. 1998)—show a strong aerosol signal that implies (given a good cloud algorithm) that aerosols can be retrieved from GridSat.

GridSat data also have the potential to help accurately determine shortwave and longwave radiative fluxes at the regional to global scale. The Earth's surface albedo is a key terrestrial variable in these flux calculations. While surface albedo data are available from the Moderate Resolution Imaging Spectroradiometer (MODIS) sensor since 2000 (Schaaf et al. 2002), long-term surface albedo data products that cover multiple decades previously could only rely on operational weather satellites that were not designed for climate monitoring. The potential to derive global maps of surface albedo from mosaics of geostationary observations has been shown by Govaerts et al. (2008), and the GridSat data might be used for the retrieval of global fields of surface albedo in this way.

The water vapor channel provides information on energetics of the upper troposphere. The channel is sensitive to a broad region of upper tropospheric humidity that can provide information on the distribution and transport of water vapor in the troposphere (Soden and Bretherton 1993; Tian et al. 2004). This channel also has the potential to provide information on water vapor entering the stratosphere (Schmetz et al. 1997) via overshooting convective clouds. In such cases, the water vapor channel can be warmer than the IR channel for convection that penetrates the tropopause. GridSat data—in providing global coverage for both channels—have the potential to help monitor the transport of water vapor.
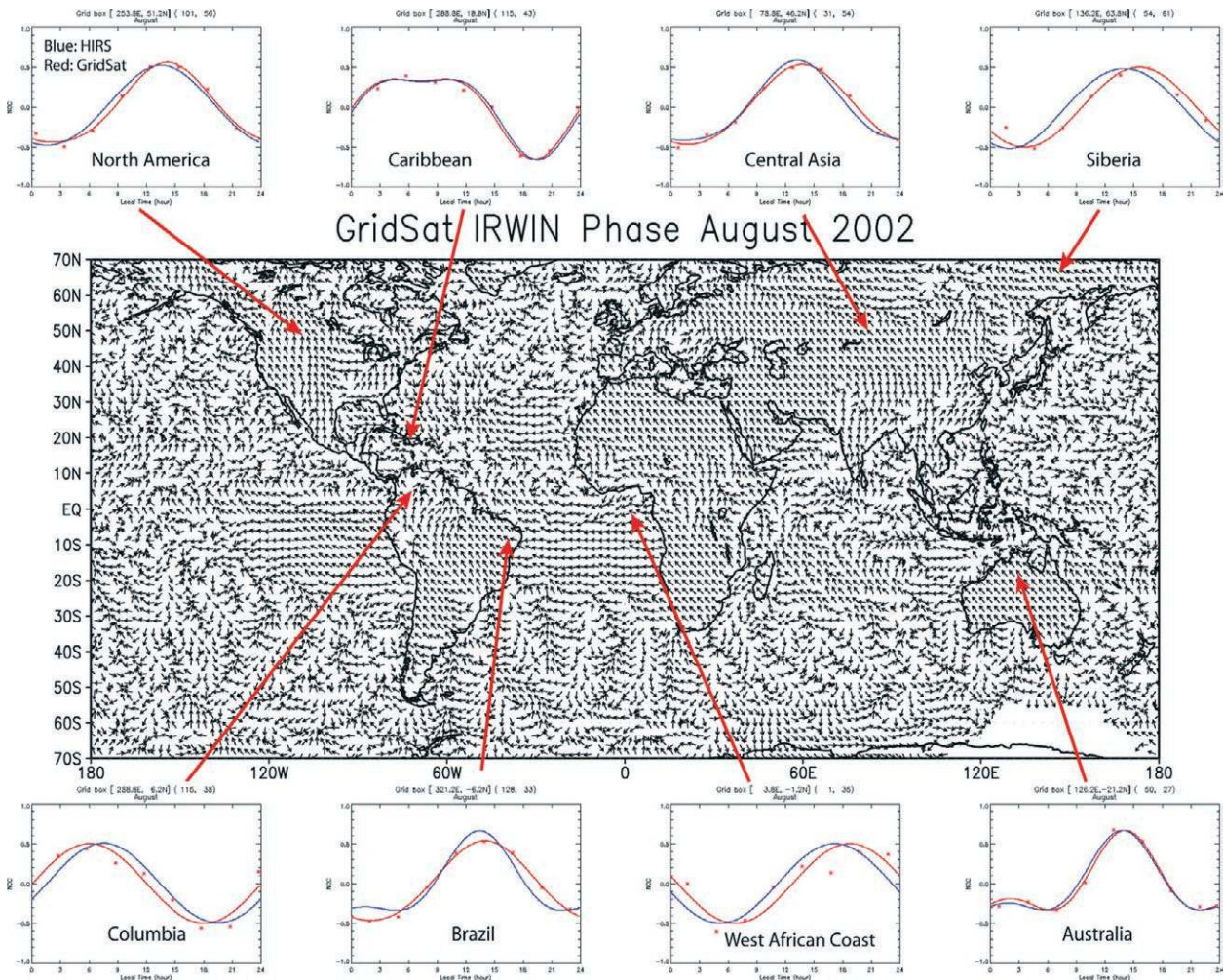
FIG. 8. Comparison of diurnal OLR models from the HIRS climatology and GridSat for August 2002. The GridSat OLR helps to verify the representativeness of the climatological OLR diurnal models used in the production of the HIRS OLR climate data record. The arrows in the central panel indicate the phases of the OLR diurnal models with the 1200 local time pointing north, running counterclockwise. The surrounding plots compare the diurnal models for selected regions with distinctively different types of diurnal variations. The mean values of GridSat OLR in each diurnal plot were adjusted to those of the HIRS to aid visual comparison.

DATASET IMPROVEMENTS. Given the widespread use of GridSat data, efforts are underway to further improve the dataset. The ISCCP project is revamping software processing to produce higher-resolution cloud products based on ISCCP B1 data. As part of this work, the pixel-level cloud mask will be incorporated into GridSat, providing information on the presence of clouds in the GridSat data.

Furthermore, the use of GridSat data by non–satellite experts suggests that a similar remapping of other satellite data would benefit more scientists. For example, instruments on polar-orbiting satellites could be remapped in a similar way. This would make data—such as that from the Advanced Very High Resolution Radiometer (AVHRR), HIRS, and other instruments—more widely available to a broad base of users.

In the future, the GridSat data will incorporate better calibration as it becomes available. In particular, the World Meteorological Organization (WMO) Global Space-Based Inter Calibration System (GSICS) is working to intercalibrate sensors on all meteorological satellites. However, the initial GSICS priority is to process operational sensors. Furthermore, their current method is to calibrate against space-based hyperspectral radiometers, thus limiting their reprocessing efforts to starting in 2002. The GSICS effort to recalibrate historical sensors (prior to 2002) has not yet begun. Nonetheless, the GridSat dataset will be reprocessed as needed to be consistent with GSICS and the NOAA CDR program.

Finally, the observations that comprise the GridSat data are being revised. The visible and water vapor

radiances will soon be intercalibrated. The IR satellite view zenith angle correction could be improved as well because the current algorithm (Joyce et al. 2001) was developed for satellites in use in 2000 (*GOES-8* and *-10*, *GMS-5*, *Meteosat-5* and *-7*). However, the corrections are likely satellite dependent, particularly because the older satellites had more water vapor contamination in the infrared window channels. An updated satellite zenith angle correction that is satellite dependent would decrease the remnant seams still apparent in GridSat IR data.

SUMMARY. Geostationary satellites have now been providing weather data for 50 years. Much of these data have been neglected by climate observation studies due to difficulties with calibration and data processing over such a long period. Collection and data ownership rights were spread out across several international agencies. The ISCCP project is overcoming these barriers and this paper has presented details on the most up-to-date and easily accessible global satellite record: GridSat.

This new record provides equal-angle gridded uniform observations of brightness temperatures every 3 h from 1980 to the present for most of the globe. We have demonstrated the multiple and diverse uses of the data for climate analysis made possible by GridSat data—from predicting drought and food security in Africa to the detailed and historical tracking of hurricanes. This only touches on some of the potential uses of GridSat. Accurate records of global atmospheric fields are essential for future research on climate change as well as the understanding of the planet's meteorology.

By reconstructing past satellite data and combining them with current satellite observations, a seamless data record has been obtained for the study of Earth's atmospheric state. In addition, GridSat has given a wide range of users very easy access to this new data record. Development of GridSat will continue, focusing on improving the current data files and supporting more applications.

REFERENCES

Adler, R. F., and Coauthors, 2003: The version-2 Global Precipitation Climatology Project (GPCP) monthly precipitation analysis (1979–present). *J. Hydrometeor.,* **4,** 1147–1167.

Ba, M. B., and A. Gruber, 2001: GOES Multispectral Rainfall Algorithm (GMSRA). *J. Appl. Meteor.,* **40,** 1500–1514.

Bain, C. L., G. Magnusdottir, P. Smyth, and H. Stern, 2010: Diurnal cycle of the intertropical convergence zone in the east Pacific. *J. Geophys. Res.,* **115,** D23116, doi:10.1029/2010JD014835.

——, J. De Paz, J. Kramer, G. Magnusdottir, P. Smyth, H. Stern, and C.-C. Wang, 2011: Detecting the ITCZ in instantaneous satellite data using spatial–temporal statistical modeling: ITCZ climatology in the east Pacific. *J. Climate,* **24,** 216–230.

Bourassa, M. A., and K. McBeth-Ford, 2010: Uncertainty in scatterometer-derived vorticity. *J. Atmos. Oceanic Technol.,* **27,** 594–603.

Cao, C., M. Goldberg, and L. Wang, 2009: Spectral bias estimation of historical HIRS using IASI observations for improved fundamental climate data records. *J. Atmos. Oceanic Technol.,* **26,** 1378–1387.

Desormeaux, Y., W. B. Rossow, C. L. Brest, and G. G. Campbell, 1993: Normalization and calibration of geostationary satellite radiances for the International Satellite Cloud Climatology Project. *J. Atmos. Oceanic Technol.,* **10,** 304–325.

Dvorak, V. F., 1975: Tropical cyclone intensity analysis and forecasting from satellite imagery. *Mon. Wea. Rev.,* **103,** 420–430.

——, 1984: Tropical cyclone intensity analysis using satellite data. NOAA Tech. Rep. NESDIS 11, 47 pp.

Elsner, J. B., J. P. Kossin, and T. H. Jagger, 2008: The increasing intensity of the strongest tropical cyclones. *Nature,* **455,** 92–95.

Environmental Protection Agency, 2008: Model-based analysis and tracking of airborne mercury emissions to assist in watershed planning. U.S. EPA, 350 pp. [Available online at www.epa.gov/owow/tmdl/pdf/final300report_10072008.pdf.]

Foley, G. R., and B. N. Hanstrum, 1994: The capture of tropical cyclones by cold fronts off the west coast of Australia. *Wea. Forecasting,* **9,** 577–592.

Funk, C., J. C. Michaelsen, and M. Marshall, 2011: Mapping recent decadal climate variations in Eastern Africa and the Sahel. *Remote Sensing of Drought: Innovative Monitoring Approaches,* B. Wardlow, and M. Anderson, Eds., Taylor and Francis, in press.

Gierach, M. M., M. A. Bourassa, P. Cunningham, J. J. O'Brien, and P. D. Reasor, 2007: Vorticity-based

detection of tropical cyclogenesis. *J. Appl. Meteor. Climatol.,* **46,** 1214–1229.

Govaerts, Y. M., A. Lattanzio, M. Taberner, and B. Pinty, 2008: Generating global surface albedo products from multiple geostationary satellites. *Remote Sens. Environ.,* **112,** 2804–2816.

Guentzel, J. L., W. M. Landing, G. A. Gill, and C. D. Pollman, 2001: Processes influencing rainfall deposition of mercury in Florida. *Environ. Sci. Technol.,* **35,** 863–873.

Hart, R. E., and J. L. Evans, 2001: A climatology of the extratropical transition of Atlantic tropical cyclones. *J. Climate,* **14,** 546–564.

Hennon, C. C., and J. S. Hobgood, 2003: Forecasting tropical cyclogenesis over the Atlantic basin using large-scale data. *Mon. Wea. Rev.,* **131,** 2927–2940.

——, C. N. Helms, K. R. Knapp, and A. R. Bowen, 2011: An objective algorithm for detecting and tracking tropical cloud clusters: Implications for tropical cyclogenesis prediction. *J. Atmos. Oceanic Technol.,* in press.

Holben, B. N., and Coauthors, 1998: AERONET—A federated instrument network and data archive for aerosol characterization. *Remote Sens. Environ.,* **66,** 1–16.

Holmes, C. D., E. S. Corbitt, D. J. Jacob, L. T. Murray, H. E. Fuelberg, and S. D. Rudlosky, 2008: Mercury deposition to the Gulf Coast region from deep convection and long-range atmospheric transport. *Eos, Trans. Amer. Geophys. Union*, **89** (Fall Meeting Suppl.), Abstract A53D-0308.

Huffman, G. J., R. F. Adler, M. M. Morrissey, D. T. Bolvin, S. Curtis, R. Joyce, B. McGavock, and J. Susskind, 2001: Global precipitation at one-degree daily resolution from multisatellite observations. *J. Hydrometeor.,* **2,** 36–50.

Janowiak, J. E., R. J. Joyce, and Y. Yarosh, 2001: A real-time global half-hourly pixel-resolution infrared dataset and its applications. *Bull. Amer. Meteor. Soc.,* **82,** 205–217.

Jones, S. C., and Coauthors, 2003: The extratropical transition of tropical cyclones: Forecast challenges, current understanding, and future directions. *Wea. Forecasting,* **18,** 1052–1092.

Joyce, R., J. Janowiak, and G. Huffman, 2001: Latitudinally and seasonally dependent zenith-angle corrections for geostationary satellite IR brightness temperatures. *J. Appl. Meteor.,* **40,** 689–703.

——, ——, P. A. Arkin, and P. Xie, 2004: CMORPH: A method that produces global precipitation estimates from passive microwave and infrared data at high spatial and temporal resolution. *J. Hydrometeor.,* **5,** 487–503.

Klein, P. M., P. A. Harr, and R. L. Elsberry, 2000: Extratropical transition of western North Pacific tropical cyclones: An overview and conceptual model of the transformation stage. *Wea. Forecasting,* **15,** 373–395.

Knapp, K. R., 2002: Quantification of aerosol signal in *GOES-8* visible imagery over the U.S. *J. Geophys. Res.,* **107,** 4426, doi:10.1029/2001JD002001.

——, 2008a: Calibration of long-term geostationary infrared observations using HIRS. *J. Atmos. Oceanic Technol.,* **25,** 183–195.

——, 2008b: Scientific data stewardship of International Satellite Cloud Climatology Project B1 global geostationary observations. *J. Appl. Remote Sens.,* **2,** 023548, doi:10.1117/1.3043461.

——, and J. P. Kossin, 2007: New global tropical cyclone data from ISCCP B1 geostationary satellite observations. *J. Appl. Remote Sens.,* **1,** 013505, doi:10.1117/1.2712816.

——, J. J. Bates, and B. Barkstrom, 2007: Scientific data stewardship: Lessons learned from a satellite data rescue effort. *Bull. Amer. Meteor. Soc.,* **88,** 1359–1361.

——, M. C. Kruk, D. H. Levinson, H. J. Diamond, and C. J. Neumann, 2010: The International Best Track Archive for Climate Stewardship (IBTrACS): Centralizing tropical cyclone best-track data. *Bull. Amer. Meteor. Soc.,* **91,** 363–376.

Kossin, J. P., J. A. Knaff, H. I. Berger, D. C. Herndon, T. A. Cram, C. S. Velden, R. J. Murnane, and J. D. Hawkins, 2007a: Estimating hurricane wind structure in the absence of aircraft reconnaissance. *Wea. Forecasting,* **22,** 89–101.

——, K. R. Knapp, D. J. Vimont, R. J. Murnane, and B. A. Harper, 2007b: A globally consistent reanalysis of hurricane variability and trends. *Geophys. Res. Lett.,* **34,** L04815, doi:10.1029/2006GL028836.

Lee, C. S., 1989: Observational analysis of tropical cyclogenesis in the western North Pacific. Part I: Structural evolution of cloud clusters. *J. Atmos. Sci.,* **46,** 2580–2598.

Lee, H.-T., A. K. Heidinger, A. Gruber, and R. G. Ellingson, 2004: The HIRS outgoing longwave radiation product from hybrid polar and geosynchronous satellite observations. *Adv. Space Res.,* **33,** 1120–1124.

——, A. Gruber, R. G. Ellingson, and I. Laszlo, 2007: Development of the HIRS outgoing longwave radiation climate data set. *J. Atmos. Oceanic Technol.,* **24,** 2029–2047.

Lindberg, S., and Coauthors, 2007: A synthesis of progress and uncertainties in attributing the sources of mercury in deposition. *Ambio,* **36,** 19–33.

Loew, A., and Y. Govaerts, 2010: Towards multidecadal consistent Meteosat surface albedo time series. *Remote Sens.,* **2,** 957–967.

Magnusdottir, G., and C.-C. Wang, 2008: Intertropical convergence zones during the active season in daily data. *J. Atmos. Sci.,* **65,** 2425–2436.

Mercury Deposition Network, 2006: National Atmospheric Deposition Program 2005 Annual Summary. 16 pp. [Available online at http://nadp.sws.uiuc.edu/lib/data/2005as.pdf.]

Mergler, D., H. A. Anderson, L. H. M. Chan, K. R. Mahaffey, M. Murray, M. Sakamoto, and A. H. Stern, 2007: Methylmercury exposure and health effects in humans: A worldwide concern. *Ambio,* **36,** 3–11.

National Research Council, 2004: Climate data records from environmental satellites. 136 pp. [Available online at www.nap.edu/catalog/10944.html.]

Rew, R., and G. Davis, 1990: NetCDF: An interface for scientific data access. *IEEE Comp. Graphics Appl.,* **10,** 76–82.

Reynolds, R. W., N. A. Rayner, T. M. Smith, D. C. Stokes, and W. Wang, 2002: An improved in situ and satellite SST analysis for climate. *J. Climate,* **15,** 1609–1625.

Schaaf, C. B., and Coauthors, 2002: First operational BRDF, albedo nadir reflectance products from MODIS. *Remote Sens. Environ.,* **83,** 135–148.

Scheuhammer, A. M., M. W. Meyer, M. B. Sandheinrich, and M. W. Murray, 2007: Effects of environmental methylmercury on the health of wild birds, mammals, and fish. *Ambio,* **36,** 12–19.

Schmetz, J., S. A. Tjemkes, M. Gube, and L. van de Berg, 1997: Monitoring deep convection and convective overshooting with METEOSAT. *Adv. Space Res.,* **19,** 433–441.

Selin, N. E., and D. J. Jacob, 2008: Seasonal and spatial patterns of mercury wet deposition in the United States: Constraints on the contribution from North American anthropogenic sources. *Atmos. Environ.,* **42,** 5193–5204.

Sharp, R. J., M. A. Bourassa, and J. J. O'Brien, 2002: Early detection of tropical cyclones using SeaWinds-derived vorticity. *Bull. Amer. Meteor. Soc.,* **83,** 879–889.

Shi, L., J. J. Bates, and C. Cao, 2008: Scene radiance-dependent intersatellite biases of HIRS longwave channels. *J. Atmos. Oceanic Technol.,* **25,** 2219–2229.

Sinclair, M. R., 2002: Extratropical transition of southwest Pacific tropical cyclones. Part I: Climatology and mean structure changes. *Mon. Wea. Rev.,* **130,** 590–609.

Soden, B. J., and F. P. Bretherton, 1993: Upper tropospheric relative humidity from the GOES 6.7-μm channel: Method and climatology for July 1987. *J. Geophys. Res.,* **98,** 16669–16688.

Soler, T., and D. W. Eisemann, 1994: Determination of look angles to geostationary communication satellites. *J. Surv. Eng. ACSE,* **120,** 115–127.

Tian, B. J., B. J. Soden, and X. Q. Wu, 2004: Diurnal cycle of convection, clouds, and water vapor in the tropical upper troposphere: Satellites versus a general circulation model. *J. Geophys. Res.,* **109,** D10101, doi:10.1029/2003JD004117.

Turk, F. J., and S. D. Miller, 2005: Toward improved characterization of remotely sensed precipitation regimes with MODIS/AMSR-E blended data techniques. *IEEE Trans. Geosci. Remote Sens.,* **43,** 1059–1069.

Waliser, D. E., and C. Gautier, 1993: A satellite-derived climatology of the ITCZ. *J. Climate,* **6,** 2162–2174.

Wang, C.-C., and G. Magnusdottir, 2006: The ITCZ in the central and eastern Pacific on synoptic time scales. *Mon. Wea. Rev.,* **134,** 1405–1421.

Zender, C. S., 2008: Analysis of self-describing gridded geoscience data with netCDF operators (NCO). *Environ. Modell. Software,* **23,** 1338–1342.